Reprinted from

CMES

Computer Modeling in Engineering & Sciences

Founder and Editor-in-Chief:
Satya N. Atluri

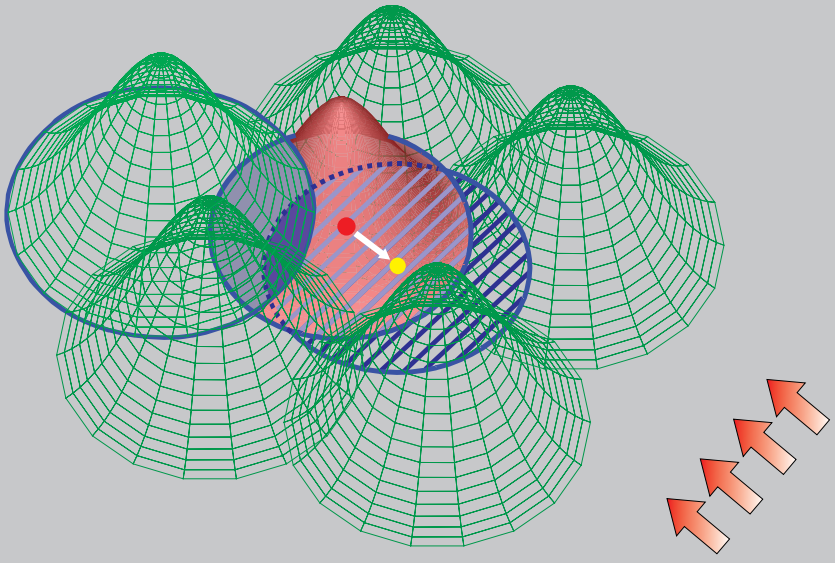

ISSN: 1526-1492 (print)
ISSN: 1526-1506 (on-line)

Tech Science Press

 CMES, vol.64, no.3, pp.267-297, 2010

The MLPG for Bending of Electroelastic Plates

J. Sladek[1], V. Sladek[1], P. Stanak[1] and E. Pan[2]

Abstract: The plate equations are obtained by means of an appropriate expansion of the mechanical displacement and electric potential in powers of the thickness coordinate in the variational equation of electroelasticity and integration through the thickness. The appropriate assumptions are made to derive the uncoupled equations for the extensional and flexural motion. The present approach reduces the original 3-D plate problem to a 2-D problem, with all the unknown quantities being localized in the mid-plane of the plate. A meshless local Petrov-Galerkin (MLPG) method is then applied to solve the problem. Nodal points are randomly spread in the mid-plane of the plate and each node is surrounded by a circular subdomain. The weak forms for the governing equations on subdomains with appropriate test functions are applied to derive local integral equations. The meshless approximation based on the moving least-squares (MLS) method is employed for the implementation. After performing the spatial MLS approximation, a system of ordinary differential equations for the nodal unknowns is obtained. The corresponding system of ordinary differential equations of the second order resulting from the equations of motion is solved by the Houbolt finite-difference scheme as a time-stepping method.

Keywords: Local integral equations, Kirchhoff theory, MLS approximation, Houbolt method, piezoelectric material, orthotropic properties

1 Introduction

Piezoelectric materials are considered as smart materials since they have a capability of converting the energy from one type to other between electric, and mechanical (Berlingcourt et al. 1964; Landau et al. 1984). Such materials combine superior mechanical properties of composite materials, as well as incorporate

[1] Institute of Construction and Architecture, Slovak Academy of Sciences, 84503 Bratislava, Slovakia

[2] Computer Modeling and Simulation Group, Department of Civil Engineering, University of Akron, Akron, OH 44325-3905, USA

inherent capability to sense and adapt their static and dynamic response. Many piezoelectric components have plate-like shapes. Some of these components like resonators and filters are used for the purpose of frequency control. Several versions of linear piezoelectric plate theories for these applications were derived by Tiersten and Mindlin (1962), Mindlin (1972), Lee et al. (1987) and Batra & Vidoli (2002). The literature on higher-order theories of piezoelectric plates has been summarized in a review article by Wang and Yang (2000). There have been many theories and models proposed for analysis of laminated composite plates containing active and passive piezoelectric layers (Lammering 1991; Lee and Moon 1990; Lee 1990; Tzou and Tseng 1990; Saravanos et al. 1997). Analytical solutions of piezoelectric plates are available only for simple boundary conditions due to the high mathematical complexity. Vel and Batra (2000) presented an analytical solution for multilayered piezoelectric plates in terms of the double Fourier series to handle more general boundary conditions at the edges.

Advanced numerical methods are required since the electric and mechanical fields are coupled. Besides the well established finite element method (FEM), the boundary element method (BEM) provides an efficient and popular alternative to the FEM. The conventional BEM is accurate and efficient for many engineering problems. However, it requires the availability of the fundamental solutions or Green's functions to the governing partial differential equations (PDE). The material anisotropy increases the number of elastic constants in Hooke's law, and hence makes the construction of the fundamental solutions cumbersome. The BEM up to date has not been applied to a piezoelectric plate bending problem. There is no particular difficulty in applying FEM to piezoelectric plates except, that the material is highly anisotropic and electromechanical coupling needs to be considered (Lerch 1990;Yong and Stewart 1991). However, the FEM has some drawbacks. The elimination of shear locking in thin walled structures by FEM is difficult and the developed techniques are less accurate. In the conventional discretization methods there is a discontinuity of secondary fields (gradients of primary fields) on the interface of elements. Meshless methods for solving PDE in physics and engineering sciences are a powerful new alternative to the traditional mesh-based techniques. Focusing only on nodes or points instead of elements used in the conventional FEM or BEM, meshless approaches have certain advantages. The moving least squares (MLS) approximation is generally considered as one of many schemes to interpolate discrete data with a reasonable accuracy. The smoothness of the shape functions is determined by that of the basis functions and of the weight functions. Since the order of the continuity of shape functions, being given by the minimum of the orders of continuity of the basis and weight functions, can be easily tuned. Although the MLS approximations showed in many applications excellent convergence of numerical

results, it has not been applied to piezoelectric plate problems up to date.

One of the most rapidly developed meshfree methods is the meshless local Petrov-Galerkin (MLPG) method. The MLPG method has attracted much attention during the past decade [Atluri and Zhu, 1998; Atluri at al. 2000; Atluri, 2004; Han et al., 2005; Mikhailov, 2002; Sellountos et al., 2005; Liu et al., 2006; Vavourakis and Polyzos, 2007] for many problems of continuum mechanics. A variety of meshless methods has been proposed so far with some of them being applied to piezoelectric and magnetoelectroelastic problems (Liu et al. 2002; Ohs and Aluru 2001; Sladek et al. 2006a, 2007a, 2008). The MLPG method with a Heaviside step function as the test functions [Atluri et al. (2003); Sladek et al., (2004)] was been applied to solve two-dimensional (2-D) homogeneous and continuously nonhomogeneous piezoelectric solids [Sladek et al., (2007b)]. The MLPG has been successfully applied also to plate problems. Long and Atluri (2002) applied the meshless local Petrov Galerkin method to solve the bending problem of a thin plate. Later, the MLPG method has been applied to Reissner-Mindlin plates and shells under dynamic load by Sladek et al. (2006b, 2007c). Soric et al. (2004) have performed a three-dimensional (3-D) analysis of thick plates, where a plate is divided by small cylindrical subdomains for which the MLPG is applied. Qian et al. (2004) extended the MLPG for 3-D deformations in thermoelastic bending of functionally graded isotropic plates.

In this paper, we will present for the first time a meshless method based on the local Petrov-Galerkin weak-form to solve dynamic problems for piezoelectric plates. The plate equations (Tiersten 1969, Yang 1999) are obtained by means of an appropriate expansion of the mechanical displacement and electric potential in powers of the thickness coordinate in the variational equation of electroelasticity and integration through the thickness. The power expansion contains terms up to cubic in the electric field and linear in the mechanical variables. Since only the lowest frequency approximations are considered, the appropriate assumptions are made and the uncoupled equations of the extensional and flexural motion are obtained (Yang 1999). The present approach reduces the original 3-D plate problem to a 2-D problem. All unknown quantities are localized in the mid-plane of the plate. The weak-forms for the governing partial differential equations on small subdomains with appropriate test functions are applied to derive local integral equations. Applying the Gauss divergence theorem to the weak-forms, the order of derivatives in governing equations is decreased. The spatial variations of the displacements and electric potential are approximated by the moving least-squares scheme (MLS) (Atluri 2004). After performing the spatial MLS approximation, a system of ordinary differential equations for certain nodal unknowns is obtained. Then, the system of the ordinary differential equations of the second order resulting from the

equations of motion is solved by the Houbolt finite-difference scheme (Houbolt 1950) as a time-stepping method.

2 Basic equations

Consider an anisotropic piezoelectric plate of constant thickness $2h$, with the mean surface occupying the domain Ω in the plane (x_1, x_2). The constitutive relations represent the coupling of the mechanical and the electrical fields. The constitutive equations for the stress σ_{ij} and electric displacement D_i can be written as [Parton and Kudryavtsev (1988)]

$$\sigma_{ij}(\mathbf{x},x_3) = c_{ijkl}(\mathbf{x},x_3)\varepsilon_{kl}(\mathbf{x},x_3) - e_{kij}(\mathbf{x},x_3)E_k(\mathbf{x},x_3), \tag{1}$$

$$D_j(\mathbf{x},x_3) = e_{jkl}(\mathbf{x},x_3)\varepsilon_{kl}(\mathbf{x},x_3) + k_{jk}(\mathbf{x},x_3)E_k(\mathbf{x},x_3), \tag{2}$$

where $c_{ijkl}(\mathbf{x},x_3)$, $e_{jkl}(\mathbf{x},x_3)$ and $k_{jk}(\mathbf{x},x_3)$ are the elastic, piezoelectric and dielectric material tensors in a continuously nonhomogeneous piezoelectric medium, respectively, and the in-plane vector $\mathbf{x}$ is represented by the Cartesian components x_α, $(\alpha = 1, 2)$, while latin indices take values 1,2,3. The strain tensor ε_{ij} and the electric field vector E_j are related to the displacements u_i and the electric potential ψ by

$$\varepsilon_{ij} = \frac{1}{2}\left(u_{i,j} + u_{j,i}\right), \tag{3}$$

$$E_j = -\psi_{,j}. \tag{4}$$

Polarized ceramics are transversely isotropic. For ceramics poled in the x_3 direction, the constitutive equations (1) and (2) are expressed by

$$\begin{bmatrix}\sigma_{11}\\ \sigma_{22}\\ \sigma_{33}\\ \sigma_{23}\\ \sigma_{13}\\ \sigma_{12}\end{bmatrix} = \begin{bmatrix} c_{11} & c_{12} & c_{13} & 0 & 0 & 0\\ c_{12} & c_{22} & c_{23} & 0 & 0 & 0\\ c_{13} & c_{23} & c_{33} & 0 & 0 & 0\\ 0 & 0 & 0 & c_{44} & 0 & 0\\ 0 & 0 & 0 & 0 & c_{44} & 0\\ 0 & 0 & 0 & 0 & 0 & c_{66}\end{bmatrix}\begin{bmatrix}\varepsilon_{11}\\ \varepsilon_{22}\\ \varepsilon_{33}\\ 2\varepsilon_{23}\\ 2\varepsilon_{13}\\ 2\varepsilon_{12}\end{bmatrix} - \begin{bmatrix} 0 & 0 & e_{31}\\ 0 & 0 & e_{31}\\ 0 & 0 & e_{33}\\ 0 & e_{15} & 0\\ e_{15} & 0 & 0\\ 0 & 0 & 0\end{bmatrix}\begin{bmatrix}E_1\\ E_2\\ E_3\end{bmatrix}$$

$$= [\mathbf{C}][\varepsilon] - [\mathbf{e}][\mathbf{E}], \tag{5}$$

$$\begin{bmatrix} D_1 \\ D_2 \\ D_3 \end{bmatrix} = \begin{bmatrix} 0 & 0 & 0 & 0 & e_{15} & 0 \\ 0 & 0 & 0 & e_{15} & 0 & 0 \\ e_{31} & e_{31} & e_{33} & 0 & 0 & 0 \end{bmatrix} \begin{bmatrix} \varepsilon_{11} \\ \varepsilon_{22} \\ \varepsilon_{33} \\ 2\varepsilon_{23} \\ 2\varepsilon_{13} \\ 2\varepsilon_{12} \end{bmatrix} + \begin{bmatrix} k_{11} & 0 & 0 \\ 0 & k_{22} & 0 \\ 0 & 0 & k_{33} \end{bmatrix} \begin{bmatrix} E_1 \\ E_2 \\ E_3 \end{bmatrix}$$

$$= [\mathbf{G}][\varepsilon] + [\mathbf{k}][\mathbf{E}]. \quad (6)$$

The governing equations for piezoelectric solids are given by the equations of motion for the mechanical displacements and by the first Maxwell equation for the vector of electric displacements [Parton and Kudryavtsev (1988)]

$$\sigma_{ij,j} + X_i = \rho \ddot{u}_i, \quad D_{j,j} - R = 0, \quad (7)$$

where $\ddot{u}_i$, X_i , R and ρ denote the acceleration, body force vector, volume density of free charges and mass density, respectively. Further, we assume vanishing body forces and volume density of free charges.

Following the well known approach [Reddy (2004), Batra and Vidoli (2002)] for plate and shell structures, the primary fields are represented as products of in-plane quantities varying in (x_1, x_2, t) and polynomial terms varying x_3 direction. This assumption reduces original 3-D problem to 2-D one with more unknown quantities. The idea is leading to the derivation of 2-D governing equations for the mid-plane of the plate. For this purpose, we shall consider the governing equations in the variational form with integrating through the plate thickness

$$\int_{-h}^{h} (\sigma_{ik,i} - \rho \ddot{u}_k) \delta u_k dx_3 = 0, \quad \int_{-h}^{h} D_{j,j} \delta \psi dx_3 = 0. \quad (8)$$

in which we shall assume polynomial expansions for the dependence of u_k and ψ on x_3. Since only the lowest frequency approximations are of interest here, the extensional and flexural deformations are uncoupled for thin plates. Then, one can use truncated series [Yang (1999)]

$$u_k(\mathbf{x}, x_3, t) = u_k^{(0)}(\mathbf{x}, t) + x_3 u_k^{(1)}(\mathbf{x}, t) + x_3^2 u_k^{(2)}(\mathbf{x}, t), \quad (9a)$$

$$\psi(\mathbf{x}, x_3, t) = \psi^{(0)}(\mathbf{x}, t) + \frac{x_3}{2h} \psi^{(1)}(\mathbf{x}, t) + \left(\frac{x_3^2}{h^2} - 1 \right) \psi^{(2)}(\mathbf{x}, t)$$

$$+ \frac{x_3}{h} \left(\frac{x_3^2}{h^2} - 1 \right) \psi^{(3)}(\mathbf{x}, t). \quad (9b)$$

Since in an electroded region of the plate, the potential difference, or voltage, across the electrode is independent of position in the plate, the electric potentials $\psi^{(0)}$ and $\psi^{(1)}$ must be independent of the coordinates x_α (α = 1, 2). However, in an unelectroded region $\psi^{(0)}$ and $\psi^{(1)}$ are in general, functions of x_α. That is why a special rearrangement is employed in the expansion series (9b).

In view of eqs. (9), the governing equations (8) become

$$\sum_{n=0}^{2} \delta u_k^{(n)}(\mathbf{x},t) \int_{-h}^{h} \left(x_3^n \sigma_{\alpha k,\alpha}(\mathbf{x},x_3,t) + x_3^n \sigma_{3k,3}(\mathbf{x},x_3,t) - \rho \sum_{m=0}^{2} x_3^{n+m} \ddot{u}_k^{(m)}(\mathbf{x},t) \right) dx_3 = 0 \quad (10a)$$

$$\sum_{n=0}^{3} \delta \psi^{(n)}(\mathbf{x},t) \int_{-h}^{h} \left(X^{(n)}(x_3) D_{\alpha,\alpha}(\mathbf{x},x_3,t) + X^{(n)}(x_3) D_{3,3}(\mathbf{x},x_3,t) \right) dx_3 = 0, \quad (10b)$$

where the notations for the functions $X^{(n)}(x_3)$ are polynomial factors in (9b) and depending on x_3. Bearing in mind the definitions

$$\sigma_{ik}^{(n)} := \int_{-h}^{h} x_3^n \sigma_{ik} dx_3, \quad F_k^{(n)} := [x_3^n \sigma_{3k}]_{-h}^{h}, \quad H_{mn} := \int_{-h}^{h} x_3^{n+m} dx_3 = \left. \frac{x_3^{n+m+1}}{n+m+1} \right|_{-h}^{h},$$

$$D_k^{(n)} := \int_{-h}^{h} x_3^n D_k dx_3, \quad d_3^{(n)} := \frac{1}{2h} [x_3^n D_3]_{-h}^{h},$$

one can rewrite eqs. (10) as

$$\sum_{n=0}^{2} \delta u_k^{(n)} \left[\sigma_{\alpha k,\alpha}^{(n)} - n\sigma_{3k}^{(n-1)} + F_k^{(n)} - \rho \sum_{m=0}^{2} H_{mn} \ddot{u}_k^{(m)} \right] = 0$$

$$\delta\psi^{(0)} \left[D_{\alpha,\alpha}^{(0)} + 2h d_3^{(0)} \right] + \delta\psi^{(1)} \left[\frac{1}{2h} D_{\alpha,\alpha}^{(1)} - \frac{1}{2h} D_3^{(0)} + d_3^{(1)} \right] +$$

$$+\delta\psi^{(2)} \left[\frac{1}{h^2} D_{\alpha,\alpha}^{(2)} - \frac{2}{h^2} D_3^{(1)} + \frac{2}{h} d_3^{(2)} - \left(D_{\alpha,\alpha}^{(0)} + 2h d_3^{(0)} \right) \right] +$$

$$+\delta\psi^{(3)} \left[\frac{1}{h^3} D_{\alpha,\alpha}^{(3)} - \frac{3}{h^3} D_3^{(3)} + \frac{2}{h^2} d_3^{(3)} - \left(\frac{1}{h} D_{\alpha,\alpha}^{(1)} - \frac{1}{h} D_3^{(0)} + 2 d_3^{(1)} \right) \right] = 0,$$

hence one can get nine equations of motion and four two-dimensional electric charge equations

$$\sigma_{\alpha k,\alpha}^{(n)} - n\sigma_{3k}^{(n-1)} + F_k^{(n)} = \rho \sum_{m=0}^{2} H_{mn} \ddot{u}_k^{(m)}, \quad n = 0,1,2, \tag{11}$$

$$D_{\alpha,\alpha}^{(0)} + 2hd_3^{(0)} = 0,$$

$$\frac{1}{2h} D_{\alpha,\alpha}^{(1)} - \frac{1}{2h} D_3^{(0)} + d_3^{(1)} = 0,$$

$$\frac{1}{h^2} D_{\alpha,\alpha}^{(2)} - D_{\alpha,\alpha}^{(0)} - \frac{2}{h^2} D_3^{(1)} = 0,$$

$$\frac{1}{h^3} D_{\alpha,\alpha}^{(3)} - \frac{1}{h} D_{\alpha,\alpha}^{(1)} - \frac{3}{h^3} D_3^{(2)} + \frac{1}{h} D_3^{(0)} = 0, \tag{12}$$

where we have utilized the relationships

$$d_3^{(2)} = -\frac{h}{2} D_{a,a}^{(0)}, \quad d_3^{(3)} = \frac{h}{2} D_3^{(0)} - \frac{h}{2} D_{\alpha,\alpha}^{(1)}$$

resulting from the definition of $d_3^{(n)}$ and the first two equations in (12). Recall that

$$H_{00} = 2h, \quad H_{01} = H_{10} = 0, \quad H_{11} = \frac{2}{3}h^3, \quad H_{02} = H_{20} = \frac{2}{3}h^3,$$

$$H_{12} = H_{21} = 0, \quad H_{22} = \frac{2}{5}h^5.$$

Substituting eq. (9a) into the strain-displacement relation (3) and rearranging terms, one can write

$$\varepsilon_{ij} = \sum_{n=0}^{2} x_3^n \varepsilon_{ij}^{(n)}, \quad \varepsilon_{ij}^{(n)} = \frac{1}{2}\left[u_{i,j}^{(n)} + u_{j,i}^{(n)} + (n+1)(\delta_{i3} u_j^{(n+1)} + \delta_{j3} u_i^{(n+1)})\right]. \tag{13}$$

The electric field vector is obtained from eq. (4) on the base of approximation (9b)

$$E_\alpha = -\psi_{,\alpha} = -\psi_{,\alpha}^{(0)} - \frac{x_3}{2h}\psi_{,\alpha}^{(1)} - \left(\frac{x_3^2}{h^2} - 1\right)\psi_{,\alpha}^{(2)} - \frac{x_3}{h}\left(\frac{x_3^2}{h^2} - 1\right)\psi_{,\alpha}^{(3)} \quad \alpha = 1,2$$

$$E_3 = -\frac{1}{2h}\psi^{(1)} - \frac{2x_3}{h^2}\psi^{(2)} - \left(\frac{3x_3^2}{h^3} - \frac{1}{h}\right)\psi^{(3)}. \tag{14}$$

The term $\varepsilon_{ij}^{(2)}$ will not be needed, since we are interested in obtaining only the uncoupled equations of anisotropic extension and elementary flexure, which is possible in this lowest order approximation. Moreover, in order to complete the reduction to the elementary theory of flexure, one must take the thickness-shear plate strains $\varepsilon_{3\alpha}^{(0)}$ to vanish as in Mindlin (1955). Then, from eq. (13), one has directly

$$u_{\alpha}^{(1)} = -u_{3,\alpha}^{(0)}. \tag{15}$$

In order to eliminate the free-plate deformations $\varepsilon_{33}^{(0)} = u_3^{(1)}$, we exclude the displacements $u_3^{(1)}$. After some uncoupling assumptions on extensional and flexural deformations nine equations of motion can be reduced to two equations for the extension and one for the flexural motion [Yang (1999)]

$$\sigma_{\alpha\beta,\alpha}^{(0)} + F_{\beta}^{(0)} = 2\rho h\ddot{u}_{\beta}^{(0)}, \tag{16}$$

$$\sigma_{\alpha\beta,\alpha\beta}^{(1)} + F_{\beta,\beta}^{(1)} + F_3^{(0)} = 2\rho h\ddot{u}_3^{(0)}. \tag{17}$$

The 2-D electric charge equations (12) are unchanged after mechanical assumptions. Now, we should find constitutive equations for integral stress $\sigma_{ij}^{(n)}$and electrical displacement $D_i^{(n)}$ quantities. In view of equations (5) and (6) as well as exclusion of $\varepsilon_{ij}^{(2)}$, we obtain the integral representations of $\sigma_p^{(m)}$ and $D_j^{(m)}$

$$\sigma_p^{(m)} = \int_{-h}^{h} x_3^m \sigma_p dx_3 = \int_{-h}^{h} x_3^m c_{pq} \sum_{n=0}^{1} x_3^n \varepsilon_q^{(n)} dx_3 - \int_{-h}^{h} x_3^m (e_{\alpha p}E_{\alpha} + e_{3p}E_3) dx_3, (m = 0, 1),$$
$$(p = 1, 2, 6)$$

$$D_j^{(m)} = \int_{-h}^{h} x_3^m e_{jq} \sum_{n=0}^{1} x_3^n \varepsilon_q^{(n)} dx_3 + \int_{-h}^{h} x_3^m (k_{j\alpha}E_{\alpha} + k_{j3}E_3) dx_3, (m = 0, 1, 2, 3), (j = 1, 2, 3)$$

where the compressed matrix notations are used for the stress and strain tensors indices (the pairs of indices $ik = 11, 22, 33, 23, 13, 12$ are replaced by $p = 1, 2, 3, 4, 5, 6$, respectively). Bearing in mind equations (13) and (14) and performing integration through the plate thickness, we obtain the electroelastic plate constitutive equations in the form

$$\sigma_p^{(0)} = 2hc_{pq}\varepsilon_q^{(0)} + 2he_{\alpha p}\psi_{,\alpha}^{(0)} - \frac{4}{3}he_{\alpha p}\psi_{,\alpha}^{(2)} + e_{3p}\psi^{(1)},$$

$$\sigma_p^{(1)} = \frac{2}{3}h^3 c_{pq}\varepsilon_q^{(1)} + \frac{h^2}{3}e_{\alpha p}\psi_{,\alpha}^{(1)} - \frac{4}{15}h^2 e_{\alpha p}\psi_{,\alpha}^{(3)} + \frac{4}{3}he_{3p}\psi^{(2)} \tag{18}$$

$$D_j^{(0)} = 2he_{jq}\varepsilon_q^{(0)} - 2hk_{j\alpha}\psi_{,\alpha}^{(0)} + \frac{4}{3}hk_{j\alpha}\psi_{,\alpha}^{(2)} - k_{j3}\psi^{(1)},$$

$$D_j^{(1)} = \frac{2}{3}h^3 e_{jp}\varepsilon_p^{(1)} - \frac{1}{3}h^2 k_{j\alpha}\psi_{,\alpha}^{(1)} + \frac{4}{15}h^2 k_{j\alpha}\psi_{,\alpha}^{(3)} - \frac{4}{3}hk_{j3}\psi^{(2)},$$

$$D_j^{(2)} = \frac{2}{3}h^3 e_{jp}\varepsilon_p^{(0)} - \frac{2}{3}h^3 k_{j\alpha}\psi_{,\alpha}^{(0)} + \frac{4}{15}h^3 k_{j\alpha}\psi_{,\alpha}^{(2)} - \frac{1}{3}h^2 k_{j3}\psi^{(1)} - \frac{8}{15}h^2 k_{j3}\psi^{(3)},$$

$$D_j^{(3)} = \frac{2}{5}h^5 e_{jp}\varepsilon_p^{(1)} - \frac{1}{5}h^4 k_{j\alpha}\psi_{,\alpha}^{(1)} + \frac{4}{35}h^4 k_{j\alpha}\psi_{,\alpha}^{(3)} - \frac{4}{5}h^3 k_{j3}\psi^{(2)}. \tag{19}$$

Substituting equations (18) and (19) into the governing equations (16), (17) and (12) and considering relations (13) and (15) we obtain 7 equations for 7 variables $u_j^{(0)}$, $\psi^{(0)}$, $\psi^{(1)}$, $\psi^{(2)}$, $\psi^{(3)}$. In the next paragraph we present computational method to solve the derived governing equations.

3. Local integral equations and numerical solution

In the previous paragraph, we have derived the governing equations for piezoelectric plate bending problem which transform original 3-D problem into 2-D one. All unknown quantities are dependent only on Cartesian coordinates $\mathbf{x} = (x_1, x_2)$ in mid-plane of the plate. Instead of writing the global weak-form for the above governing equations, the MLPG method constructs a weak-form over the local fictitious subdomains such as Ω_s, which is a small region constructed for each node inside the global domain [Atluri, (2004)]. The local subdomains overlap each other, and cover the whole global domain Ω (Fig. 1). The local subdomains could be of any geometrical shape and size. In the present paper, the local subdomains are taken to be of a circular shape for simplicity. The local weak-form of the governing equation (16) can be written as

$$\int_{\Omega_s} \left[\sigma_{\alpha\beta,\alpha}^{(0)}(\mathbf{x},t) + F_\beta^{(0)}(\mathbf{x},t) - 2h\rho(\mathbf{x})\ddot{u}_\beta^{(0)}(\mathbf{x},t)\right] u_{\beta\gamma}^*(\mathbf{x})\, d\Omega = 0, \tag{20}$$

where $u_{\beta\gamma}^*(\mathbf{x})$ is the weight or test functions.

Applying the Gauss divergence theorem to the first domain integral in equation (20) one obtains

$$\int_{\partial\Omega_s^i} \sigma_{\alpha\beta}^{(0)}(\mathbf{x},t) n_\alpha(\mathbf{x}) u_{\beta\gamma}^*(\mathbf{x}) d\Gamma - \int_{\Omega_s^i} \sigma_{\alpha\beta}^{(0)}(\mathbf{x},t) u_{\beta\gamma,\alpha}^*(\mathbf{x}) d\Omega + \int_{\Omega_s^i} \left(F_\beta^{(0)} - 2h\rho\ddot{u}_\beta^{(0)}\right) u_{\beta\gamma}^*(\mathbf{x}) d\Omega = 0, \tag{21}$$

where $\partial\Omega_s^i$ is the boundary of the local subdomainΩ_s^icentered at the node $\mathbf{y}^i$ and n_α is the unit outward normal vector to the boundary $\partial\Omega_s^i$. The local weak-forms

(20) and (21) are the starting point for deriving local boundary integral equations on the basis of appropriate test functions. By choosing the test function as

$$u^*_{\beta\gamma}(\mathbf{x}) = [1 - H(r - r_0)]\,\delta_{\beta\gamma}, \tag{22}$$

with $H(z)$ being the Heaviside unit step function ($H(z) = 1$ for $z > 0$, $H(z) = 0$ for $z \le 0$), $r = \sqrt{r_\alpha r_\alpha}$, $r_\alpha = x_\alpha - y^i_\alpha$ and r_0 being the radius of the circular subdomain Ω^i_s, the first domain integral in (21) is vanishing and the local integral equation can be rewritten into the form

$$\int_{\partial\Omega^i_s} \sigma^{(0)}_{\alpha\beta}(\mathbf{x},t) n_\alpha(\mathbf{x}) d\Gamma + \int_{\Omega^i_s} \left(F^{(0)}_\beta - 2h\rho \ddot{u}^{(0)}_\beta \right) d\Omega = 0, \ (\beta = 1, 2) \tag{23}$$

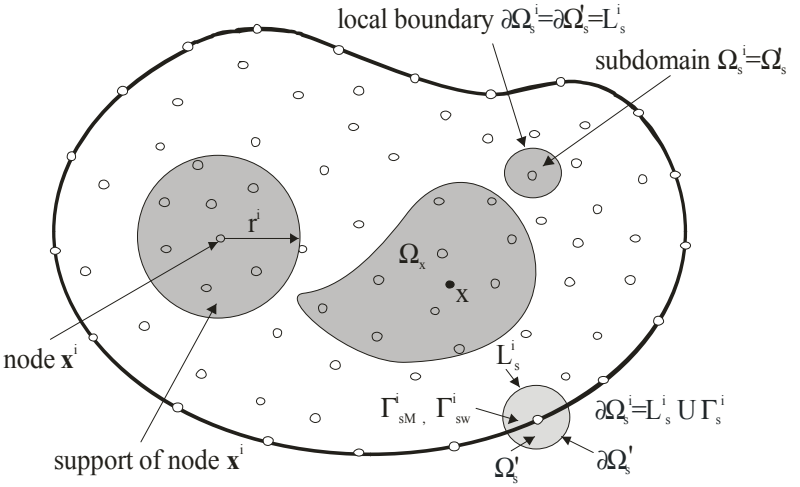

Figure 1: Local boundaries for weak formulation, the domain Ω_x for MLS approximation of the trial function, and support area of weight function around node $\mathbf{x}^i$

Similarly, one can derive the local integral equation from the governing equation (17)

$$\int_{\partial\Omega^i_s} \left(n_\beta \sigma^{(1)}_{\alpha\beta,\alpha}(\mathbf{x},t) w^*(\mathbf{x}) - n_\alpha \sigma^{(1)}_{\alpha\beta}(\mathbf{x},t) w^*_{,\beta}(\mathbf{x}) \right) d\Gamma + \int_{\Omega^i_s} \sigma^{(1)}_{\alpha\beta}(\mathbf{x},t) w^*_{,\alpha\beta}(\mathbf{x}) d\Omega +$$

$$+ \int_{\Omega^i_s} \left(F^{(1)}_{\beta,\beta}(\mathbf{x},t) + F^{(0)}_3(\mathbf{x},t) - 2h\rho \ddot{u}^{(0)}_3(\mathbf{x},t) \right) w^*(\mathbf{x}) d\Omega = 0. \tag{24}$$

Making use of the weight function as $w^*(\mathbf{x}) = (r-r_0)^\kappa$, $r = \left|\mathbf{x}-\mathbf{x}^i\right|$, then

$$w^*_{,\beta}(\mathbf{x}) = \kappa (r-r_0)^{\kappa-1} r_{,\beta},$$

$$w^*_{,\alpha\beta}(\mathbf{x}) = \kappa (r-r_0)^{\kappa-1} \left[\frac{\kappa-1}{r-r_0} r_{,\alpha} r_{,\beta} + \frac{1}{r}\left(\delta_{\alpha\beta} - r_{,\alpha} r_{,\beta}\right)\right] \tag{25}$$

and the boundary integral in the local integral equation (LIE) is missing as long as $\kappa > 1$, i.e.

$$\int\limits_{\Omega_s^i} \sigma^{(1)}_{\alpha\beta}(\mathbf{x},t) w^*_{,\alpha\beta}(\mathbf{x}) d\Omega + \int\limits_{\Omega_s^i} \left(F^{(1)}_{\beta,\beta}(\mathbf{x},t) + F^{(0)}_3(\mathbf{x},t) - 2h\rho \ddot{u}^{(0)}_3(\mathbf{x},t)\right) w^*(\mathbf{x}) d\Omega = 0. \tag{26}$$

The local weak-forms of the set of governing equations (12) for $\mathbf{x}^i \in \Omega_s^i$ after application of Gauss divergence theorem can be written as

$$\int\limits_{\partial\Omega_s^i} n_\alpha(\mathbf{x}) D^{(0)}_\alpha(\mathbf{x},t) \psi^*(\mathbf{x}) d\Gamma - \int\limits_{\Omega_s^i} D^{(0)}_\alpha(\mathbf{x},t) \psi^*_{,\alpha}(\mathbf{x}) d\Omega + \int\limits_{\Omega_s^i} 2h d^{(0)}_3(\mathbf{x},t) \psi^*(\mathbf{x}) d\Omega = 0,$$

$$\int\limits_{\partial\Omega_s^i} n_\alpha(\mathbf{x}) D^{(1)}_\alpha(\mathbf{x},t) \psi^*(\mathbf{x}) d\Gamma - \int\limits_{\Omega_s^i} D^{(1)}_\alpha(\mathbf{x},t) \psi^*_{,\alpha}(\mathbf{x}) d\Omega + \int\limits_{\Omega_s^i} \left(2h d^{(1)}_3 - D^{(0)}_3\right) \psi^*(\mathbf{x}) d\Omega = 0,$$

$$\int\limits_{\partial\Omega_s^i} n_\alpha(\mathbf{x}) \left[D^{(2)}_\alpha(\mathbf{x},t) - h^2 D^{(0)}_\alpha(\mathbf{x},t)\right] \psi^*(\mathbf{x}) d\Gamma + \int\limits_{\Omega_s^i} \left[h^2 D^{(0)}_\alpha(\mathbf{x},t) - D^{(2)}_\alpha(\mathbf{x},t)\right] \psi^*_{,\alpha}(\mathbf{x}) d\Omega - \int\limits_{\Omega_s^i} 2D^{(1)}_3(\mathbf{x},t) \psi^*(\mathbf{x}) d\Omega = 0,$$

$$\int\limits_{\partial\Omega_s^i} n_\alpha(\mathbf{x}) \left[D^{(3)}_\alpha(\mathbf{x},t) - h^2 D^{(1)}_\alpha(\mathbf{x},t)\right] \psi^*(\mathbf{x}) d\Gamma + \int\limits_{\Omega_s^i} \left[h^2 D^{(1)}_\alpha(\mathbf{x},t) - D^{(3)}_\alpha(\mathbf{x},t)\right] \psi^*_{,\alpha}(\mathbf{x}) d\Omega + \int\limits_{\Omega_s^i} \left[h^2 D^{(0)}_3(\mathbf{x},t) - 3D^{(2)}_3(\mathbf{x},t)\right] \psi^*(\mathbf{x}) d\Omega = 0. \tag{27}$$

Choosing the weight function as $\psi^*(\mathbf{x}) = [1 - H(r - r_0)]$, then

$$\psi^*(\mathbf{x})|_{\Omega_s^i \cup \partial\Omega_s^i} = 1, \quad \psi^*_{,\alpha}(\mathbf{x})\big|_{\Omega_s^i} = 0, \tag{28}$$

and the LIE become

$$\int_{\partial\Omega_s^i} n_\alpha(\mathbf{x}) D_\alpha^{(0)}(\mathbf{x},t)d\Gamma + \int_{\Omega_s^i} 2hd_3^{(0)}(\mathbf{x},t)d\Omega = 0, \tag{29}$$

$$\int_{\partial\Omega_s^i} n_\alpha(\mathbf{x}) D_\alpha^{(1)}(\mathbf{x},t)d\Gamma + \int_{\Omega_s^i} \left(2hd_3^{(1)} - D_3^{(0)}\right) d\Omega = 0, \tag{30}$$

$$\int_{\partial\Omega_s^i} n_\alpha(\mathbf{x}) \left[D_\alpha^{(2)}(\mathbf{x},t) - h^2 D_\alpha^{(0)}(\mathbf{x},t)\right] d\Gamma - \int_{\Omega_s^i} 2D_3^{(1)}(\mathbf{x},t)d\Omega = 0, \tag{31}$$

$$\int_{\partial\Omega_s^i} n_\alpha(\mathbf{x}) \left[D_\alpha^{(3)}(\mathbf{x},t) - h^2 D_\alpha^{(1)}(\mathbf{x},t)\right] d\Gamma + \int_{\Omega_s^i} \left[h^2 D_3^{(0)}(\mathbf{x},t) - 3D_3^{(2)}(\mathbf{x},t)\right] d\Omega = 0. \tag{32}$$

Again the in-plane unknowns are localized on $\partial\Omega_s^i$. Substituting constitutive equations (18) and (19) into the local integral equations (23), (26) and (29-32) and considering relations (13) and (15) we have to solve 7 equations for 7 variables $u_j^{(0)}$, $\psi^{(0)}$, $\psi^{(1)}$, $\psi^{(2)}$, $\psi^{(3)}$. For this purpose it is convenient to apply a meshless method. In general, a meshless method uses a local interpolation to represent the trial function with the values of the unknown variable (or the fictitious values) at some randomly located nodes. The moving least-squares (MLS) approximation [Lancaster and Salkauskas, 1981; Nayroles et al., 1992; Belytschko, 1996] used in the present analysis may be considered as one of such schemes.

The approximated functions for the mechanical displacements and the electric potential can be written as [Atluri, 2004]

$$\mathbf{u}^{(0)}(\mathbf{x},t) = \mathbf{\Phi}^T(\mathbf{x}) \cdot \hat{\mathbf{u}}^{(\mathbf{0})}(t) = \sum_{a=1}^{s} \phi^a(\mathbf{x}) \hat{\mathbf{u}}^{a(0)}(t), \quad \mathbf{u}^{(0)} = (u_1^{(0)}, u_2^{(0)})^T$$

$$u_3^{(0)}(\mathbf{x},t) = \sum_{a=1}^{s} \phi^a(\mathbf{x}) \hat{u}_3^{a(0)}(t)$$

$$\psi^{(n)}(\mathbf{x},t) = \sum_{a=1}^{s} \phi^a(\mathbf{x}) \hat{\psi}^{a(n)}(t), \ (n = 0, 1, 2, 3) \tag{33a}$$

where the nodal values $\hat{\mathbf{u}}^{a(0)}(t)$, $\hat{u}_3^{a(0)}(t)$ and $\hat{\psi}^{a(n)}(t)$ are fictitious parameters for the displacements and the electric potential, respectively, and $\phi^a(\mathbf{x})$ is the shape function associated with the node a. In order to decrease the order of derivatives of the shape functions (in the approximation of $\sigma_{\alpha\beta}^{(1)}$), we assume also the approximation

$$\mathbf{u}^{(1)}(\mathbf{x},t) = \sum_{a=1}^{s} \phi^a(\mathbf{x})\hat{\mathbf{u}}^{a(1)}(t), \quad \mathbf{u}^{(1)} = (u_1^{(1)}, u_2^{(1)})^T$$

with $\mathbf{u}^{(1)}(\mathbf{x},t) = -\begin{pmatrix} u_{3,1}^{(0)} \\ u_{3,2}^{(0)} \end{pmatrix}$, i.e.

$$\sum_{a=1}^{s} \phi^a(\mathbf{x})\hat{\mathbf{u}}^{a(1)}(t) = -\sum_{a=1}^{s} \mathbf{P}^a(\mathbf{x})\hat{u}_3^{a(0)}(t), \mathbf{P}^a(\mathbf{x}) = \begin{pmatrix} \phi_{,1}^a \\ \phi_{,2}^a \end{pmatrix}. \tag{33b}$$

The number of nodes s used for the approximation at the point $\mathbf{x}$ is determined by the weight functions $w^a(\mathbf{x})$. The fourth order spline-type weight function is applied in the present work

$$w^a(\mathbf{x}) = \begin{cases} 1 - 6\left(\frac{d^a}{r^a}\right)^2 + 8\left(\frac{d^a}{r^a}\right)^3 - 3\left(\frac{d^a}{r^a}\right)^4, & 0 \le d^a \le r^a \\ 0, & d^a \ge r^a \end{cases}, \ (a = 1, 2, ..., N_t) \tag{34}$$

where $d^a = \|\mathbf{x} - \mathbf{x}^a\|$, r^a is the radius of the support domain and N_t is the total number of nodal points. It is seen that the C^1-continuity is ensured over the entire domain, therefore the continuity conditions of the tractions and the electric charge are satisfied.

The stresses $\boldsymbol{\sigma}^{(0)}(\mathbf{x},t) = (\sigma_{11}^{(0)}, \sigma_{22}^{(0)}, \sigma_{12}^{(0)})^T$ and $\boldsymbol{\sigma}^{(1)}(\mathbf{x},t) = (\sigma_{11}^{(1)}, \sigma_{22}^{(1)}, \sigma_{12}^{(1)})^T$ at a boundary point $\mathbf{x} \in \partial\Omega_s$ are approximated in terms of the nodal values $\hat{\mathbf{u}}^{a(0)}(t)$, $\hat{u}_3^{a(0)}(t)$, $\hat{\psi}^{a(n)}(t)$ as follows

$$\boldsymbol{\sigma}^{(0)}(\mathbf{x},t) = 2h\mathbf{C}(\mathbf{x}) \sum_{a=1}^{s} \mathbf{B}^a(\mathbf{x})\hat{\mathbf{u}}^{a(0)}(t) + \mathbf{F}(\mathbf{x}) \sum_{a=1}^{s} \phi^a(\mathbf{x})\hat{\psi}^{a(1)}(t), \tag{35}$$

$$\boldsymbol{\sigma}^{(1)}(\mathbf{x},t) = \frac{2}{3}h^3\mathbf{C}(\mathbf{x}) \sum_{a=1}^{s} \mathbf{B}^a(\mathbf{x})\hat{\mathbf{u}}^{a(1)}(t) + \frac{4}{3}h\mathbf{F}(\mathbf{x}) \sum_{a=1}^{s} \phi^a(\mathbf{x})\hat{\psi}^{a(2)}(t), \tag{36}$$

where the matrix $\mathbf{B}^a$ is represented by the gradients of the shape functions and $\mathbf{C}$, $\mathbf{F}$ are matrices of the material coefficients

$$\mathbf{B}^a(\mathbf{x}) = \begin{bmatrix} \phi_{,1}^a & 0 \\ 0 & \phi_{,2}^a \\ \phi_{,2}^a & \phi_{,1}^a \end{bmatrix}, \quad \mathbf{C}(\mathbf{x}) = \begin{bmatrix} c_{11} & c_{12} & 0 \\ c_{12} & c_{22} & 0 \\ 0 & 0 & c_{66} \end{bmatrix}, \quad \mathbf{F}(\mathbf{x}) = \begin{bmatrix} e_{31} \\ e_{31} \\ 0 \end{bmatrix}.$$

Similarly the electrical displacements $\mathbf{D^{(n)}}(\mathbf{x},t) = (D_1^{(n)}, D_2^{(n)})^T$ can be approximated by

$$\mathbf{D}^{(0)}(\mathbf{x},t) = \mathbf{K2}(\mathbf{x}) \sum_{a=1}^{s} \mathbf{P}^a(\mathbf{x}) \left[-2h\hat{\psi}^{a(0)}(t) + \frac{4}{3}h\hat{\psi}^{a(2)}(t) \right], \tag{37}$$

$$\mathbf{D}^{(1)}(\mathbf{x},t) = \mathbf{K2}(\mathbf{x}) \sum_{a=1}^{s} \mathbf{P}^a(\mathbf{x}) \left[-\frac{h^2}{3}\hat{\psi}^{a(1)}(t) + \frac{4}{15}h^2\hat{\psi}^{a(3)}(t) \right], \tag{38}$$

$$\mathbf{D}^{(2)}(\mathbf{x},t) = \mathbf{K2}(\mathbf{x}) \sum_{a=1}^{s} \mathbf{P}^a(\mathbf{x}) \left[-\frac{2}{3}h^3\hat{\psi}^{a(0)}(t) + \frac{4}{15}h^3\hat{\psi}^{a(2)}(t) \right], \tag{39}$$

$$\mathbf{D}^{(3)}(\mathbf{x},t) = \mathbf{K2}(\mathbf{x}) \sum_{a=1}^{s} \mathbf{P}^a(\mathbf{x}) \left[-\frac{1}{5}h^4\hat{\psi}^{a(1)}(t) + \frac{4}{35}h^4\hat{\psi}^{a(3)}(t) \right], \tag{40}$$

where the matrix **K2** is defined as

$$\mathbf{K2}(\mathbf{x}) = \begin{bmatrix} k_{11} & 0 \\ 0 & k_{22} \end{bmatrix}.$$

The third component of the electrical displacement is approximated by

$$D_3^{(0)}(\mathbf{x},t) = 2h\mathbf{G}_3(\mathbf{x}) \sum_{a=1}^{s} \mathbf{B}3^a(\mathbf{x})\hat{\mathbf{u}}^{a(0)}(t) - k_{33}(\mathbf{x}) \sum_{a=1}^{s} \phi^a(\mathbf{x})\hat{\psi}^{a(1)}(t), \tag{41}$$

$$D_3^{(1)}(\mathbf{x},t) = \frac{2}{3}h^3\mathbf{G}_3(\mathbf{x}) \sum_{a=1}^{s} \mathbf{B}3^a(\mathbf{x})\hat{\mathbf{u}}^{a(1)}(t) - \frac{4}{3}hk_{33}(\mathbf{x}) \sum_{a=1}^{s} \phi^a(\mathbf{x})\hat{\psi}^{a(2)}(t), \tag{42}$$

$$\begin{aligned} D_3^{(2)}(\mathbf{x},t) = {} & \frac{2}{3}h^3\mathbf{G}_3(\mathbf{x}) \sum_{a=1}^{s} \mathbf{B}3^a(\mathbf{x})\hat{\mathbf{u}}^{a(0)}(t) \\ & - \frac{1}{15}h^2k_{33}(\mathbf{x}) \sum_{a=1}^{s} \phi^a(\mathbf{x}) \left[5\hat{\psi}^{a(1)}(t) + 8\hat{\psi}^{a(3)}(t) \right], \end{aligned} \tag{43}$$

$$D_3^{(3)}(\mathbf{x},t) = \frac{2}{5}h^5\mathbf{G}_3(\mathbf{x}) \sum_{a=1}^{s} \mathbf{B}3^a(\mathbf{x})\hat{\mathbf{u}}^{a(1)}(t) - \frac{4}{5}h^3k_{33}(\mathbf{x}) \sum_{a=1}^{s} \phi^a(\mathbf{x})\hat{\psi}^{a(2)}(t), \tag{44}$$

where

$$\mathbf{G}_3(\mathbf{x}) = (e_{31}, e_{31}),\ \mathbf{B}3^a(\mathbf{x}) = \begin{bmatrix} \phi^a_{,1} & 0 \\ 0 & \phi^a_{,2} \end{bmatrix}.$$

Then, insertion of the MLS-discretized stress fields (35), (36) and electrical displacements (37-44) into the local integral equations (23), (26) and (29-32) yields the discretized LIEs

$$2h\sum_{a=1}^{N_t}\left(\int_{\partial\Omega_s^i}\bar{\mathbf{N}}(\mathbf{x})\mathbf{C}(\mathbf{x})\mathbf{B}^a(\mathbf{x})d\Gamma\right)\hat{\mathbf{u}}^{a(0)}(t)+\sum_{a=1}^{N_t}\left(\int_{\partial\Omega_s^i}\bar{\mathbf{N}}(\mathbf{x})\mathbf{F}(\mathbf{x})\phi^a(\mathbf{x})d\Gamma\right)\hat{\psi}^{a(1)}(t)$$

$$-2h\sum_{a=1}^{N_t}\left(\int_{\Omega_s^i}\rho(\mathbf{x})\phi^a(\mathbf{x})d\Omega\right)\ddot{\hat{\mathbf{u}}}^{a(0)}(t)=0,\quad \bar{\mathbf{N}}(\mathbf{x})=\begin{pmatrix}n_1 & 0 & n_2\\ 0 & n_2 & n_1\end{pmatrix} \tag{45}$$

since $F_\beta^{(0)}=\sigma_{3\beta}\big|_{-h}^{h}=0$;

$$\frac{2}{3}h^3\sum_{a=1}^{N_t}\left(\int_{\Omega_s^i}\mathbf{W}^*(\mathbf{x})\mathbf{C}(\mathbf{x})\mathbf{B}^a(\mathbf{x})d\Omega\right)\hat{\mathbf{u}}^{a(1)}(t)$$

$$+\frac{4}{3}h\sum_{a=1}^{N_t}\left(\int_{\Omega_s^i}\mathbf{W}^*(\mathbf{x})\mathbf{F}(\mathbf{x})\phi^a(\mathbf{x})d\Omega\right)\hat{\psi}^{a(2)}(t)$$

$$-2h\sum_{a=1}^{N_t}\left(\int_{\Omega_s^i}w^*(\mathbf{x})\rho(\mathbf{x})\phi^a(\mathbf{x})d\Omega\right)\ddot{\hat{u}}_3^{a(0)}(t)+\int_{\Omega_s^i}\left[\sigma_{33}^+-\sigma_{33}^-\right]w^*(\mathbf{x})d\Omega=0,$$

$$\mathbf{W}^*(\mathbf{x})=(w^*_{,11},w^*_{,22},w^*_{,12}) \tag{46}$$

since $F_\beta^{(1)}=\left(x_3\sigma_{3\beta}\right)\big|_{-h}^{h}=0$, $F_3^{(0)}=\sigma_{33}\big|_{-h}^{h}=\sigma_{33}^+-\sigma_{33}^-$;

$$\sum_{a=1}^{s}\left(\int_{\partial\Omega_s^i}\mathbf{N}(\mathbf{x})\mathbf{K2}(\mathbf{x})\mathbf{P}^a(\mathbf{x})d\Gamma\right)\left[2h\hat{\psi}^{a(0)}(t)-\frac{4}{3}h\hat{\psi}^{a(2)}(t)\right]-\int_{\Omega_s^i}\left[D_3^+-D_3^-\right]d\Omega=0,$$

$$\mathbf{N}(\mathbf{x})=(n_1,n_2) \tag{47}$$

$$\sum_{a=1}^{N_t}\left(\int_{\partial\Omega_s^i}\mathbf{N}(\mathbf{x})\mathbf{K2}(\mathbf{x})\mathbf{P}^a(\mathbf{x})d\Gamma\right)\left[-\frac{h}{6}\hat{\psi}^{a(1)}(t)+\frac{2}{15}h\hat{\psi}^{a(3)}(t)\right]-$$

$$-\sum_{a=1}^{N_t}\left(\int_{\Omega_s^i}\mathbf{G}_3(\mathbf{x})\mathbf{B}3^a(\mathbf{x})d\Omega\right)\hat{\mathbf{u}}^{a(0)}(t)+\frac{1}{2h}\sum_{a=1}^{N_t}\left(\int_{\Omega_s^i}k_{33}(\mathbf{x})\phi^a(\mathbf{x})d\Omega\right)\hat{\psi}^{a(1)}(t)$$

$$+\frac{1}{2}\int_{\Omega_s^i}\left[D_3^+ + D_3^-\right]d\Omega = 0, \tag{48}$$

$$\sum_{a=1}^{N_t}\left(\int_{\partial\Omega_s^i}\mathbf{N}(\mathbf{x})\mathbf{K2}(\mathbf{x})\mathbf{P}^a(\mathbf{x})d\Gamma\right)\left[\frac{4}{3}h\hat{\psi}^{a(0)}(t)-\frac{16}{15}h\hat{\psi}^{a(2)}(t)\right]$$

$$-\frac{4}{3}h\sum_{a=1}^{N_t}\left(\int_{\Omega_s^i}\mathbf{G}_3(\mathbf{x})\mathbf{B}3^a(\mathbf{x})d\Omega\right)\hat{\mathbf{u}}^{a(1)}(t)+\frac{8}{3h}\sum_{a=1}^{N_t}\left(\int_{\Omega_s^i}k_{33}(\mathbf{x})\phi^a(\mathbf{x})d\Omega\right)\hat{\psi}^{a(2)}(t)$$

$$= 0, \tag{49}$$

$$h^2\sum_{a=1}^{N_t}\left(\int_{\partial\Omega_s^i}\mathbf{N}(\mathbf{x})\mathbf{K2}(\mathbf{x})\mathbf{P}^a(\mathbf{x})d\Gamma\right)\left[\frac{2}{15}\hat{\psi}^{a(1)}(t)-\frac{16}{105}\hat{\psi}^{a(3)}(t)\right]$$

$$+\frac{8}{5}\sum_{a=1}^{N_t}\left(\int_{\Omega_s^i}k_{33}(\mathbf{x})\phi^a(\mathbf{x})d\Omega\right)\hat{\psi}^{a(3)}(t)=0. \tag{50}$$

Having used 7+2 variables ($u_j^{(0)}$, $\psi^{(0)}$, $\psi^{(1)}$, $\psi^{(2)}$, $\psi^{(3)}$) + $u_\alpha^{(1)}$, we need to incorporate also eq. (33b) into the set of discretized governing equations given by (45)-(50).

Equations (45-50) are considered on the subdomains adjacent to the interior nodes $\mathbf{x}^i$ lying in the mid-plane of plate. For the source point $\mathbf{x}^i$ located on the global boundary of the mid-plane,Γ, the boundary conditions are satisfied by the collocation directly from the approximation of corresponding quantities. For in-plane deformations, the boundary conditions are prescribed in a standard way by specifying either in-plane displacements or in-plane tractions on Γ, i.e.

$u_\alpha^{(0)} = \bar{u}_\alpha$ on Γ_D, $n_\beta\sigma_{\alpha\beta}^{(0)} = \bar{t}_\alpha$ on Γ_N , with $\Gamma = \Gamma_D \cup \Gamma_N$.

In the discretized form, the in-plane boundary conditions are given as

$$\sum_{a=1}^{s}\phi^a(\mathbf{x}^i)\hat{\mathbf{u}}^{a(0)}(t)=\begin{pmatrix}\bar{u}_1\\ \bar{u}_2\end{pmatrix},$$

$$\bar{\mathbf{N}}(\mathbf{x}^i)\left[2h\mathbf{C}(\mathbf{x}^i)\sum_{a=1}^{s}\mathbf{B}^a(\mathbf{x}^i)\hat{\mathbf{u}}^{a(0)}(t)+\mathbf{F}(\mathbf{x}^i)\sum_{a=1}^{s}\phi^a(\mathbf{x}^i)\hat{\psi}^{a(1)}(t)\right]=\begin{pmatrix}\bar{t}_1\\ \bar{t}_2\end{pmatrix}.$$

If no in-plane loading is considered, then the in-plane displacements are given by gradients of transversal displacement (deflection). For simply supported plate the deflection and bending moment have to vanish at the collocation nodes $\mathbf{x}^i \in \Gamma$

$$u_3^{(0)}=0, \tag{51a}$$

$$n_\alpha n_\beta \sigma_{\alpha\beta}^{(1)}=0. \tag{51b}$$

Moreover, it can be seen that

$$\tau_\alpha u_\alpha^{(1)}=-\tau_\alpha u_{3,\alpha}^{(0)}=-\tau_\alpha\left[n_\alpha\frac{\partial u_3^{(0)}}{\partial \mathbf{n}}+\tau_\alpha\frac{\partial u_3^{(0)}}{\partial \boldsymbol{\tau}}\right]=-\frac{\partial u_3^{(0)}}{\partial \boldsymbol{\tau}}\equiv 0, \tag{51c}$$

where $\mathbf{n}$ and $\boldsymbol{\tau}$ are the normal and tangential unit vectors on the boundary contour of the plate. The last equality in (51c) results from (51a).

Substituting approximations (33) and (35) into boundary conditions (51) we obtain collocation equations for nodes on the global boundary

$$\sum_{a=1}^{s}\phi^a(\mathbf{x}^i)\hat{u}_3^{a(0)}(t)=0, \tag{52}$$

$$\mathbf{N}(\mathbf{x})\bar{\mathbf{N}}(\mathbf{x})\left[\frac{2}{3}h^3\mathbf{C}(\mathbf{x})\sum_{a=1}^{s}\mathbf{B}^a(\mathbf{x})\hat{\mathbf{u}}^{a(1)}(t)+\frac{4}{3}h\mathbf{F}(\mathbf{x})\sum_{a=1}^{s}\phi^a(\mathbf{x})\hat{\psi}^{a(2)}(t)\right]=0,\quad \mathbf{x}^i\in\Gamma \tag{53a}$$

$$\mathbf{T}(\mathbf{x}^i)\sum_{a=1}^{s}\phi^a(\mathbf{x}^i)\hat{\mathbf{u}}^{a(1)}(t)=0,\quad \mathbf{T}(\mathbf{x}^i)=(\tau_1,\tau_2). \tag{53b}$$

Collocation equations (52) and (53) represent 3 equations for three unknown mechanical quantities $u_3^{(0)}$, $u_1^{(1)}$, $u_2^{(1)}$. The clamped boundary conditions are given by vanishing deflection and rotations. Then, equations (53) are replaced by

$$\begin{pmatrix}u_1^{(1)}\\ u_2^{(1)}\end{pmatrix}=\sum_{a=1}^{s}\phi^a(\mathbf{x}^i)\hat{\mathbf{u}}^{a(1)}(t)=0. \tag{54}$$

Electrical boundary conditions are represented either by essential

$\psi^{(n)}=0$ (n = 0,1,2,3)

or by natural conditions

$$D_{\beta}^{(n)} n_{\beta} = 0.$$

In the discretized form, the boundary conditions are given as

$$\sum_{a=1}^{s} \phi^{a}(\mathbf{x}^{i}) \hat{\psi}^{a(n)}(t) = 0, \ (n = 0,1,2,3) \tag{55}$$

or

$$\mathbf{N}(\mathbf{x}^{i})\mathbf{K2}(\mathbf{x}^{i}) \sum_{a=1}^{s} \mathbf{P}^{a}(\mathbf{x}^{i}) \left[-2h\hat{\psi}^{a(0)}(t) + \frac{4}{3} h \hat{\psi}^{a(2)}(t) \right] = 0, \tag{56}$$

$$\mathbf{N}(\mathbf{x}^{i})\mathbf{K2}(\mathbf{x}^{i}) \sum_{a=1}^{s} \mathbf{P}^{a}(\mathbf{x}^{i}) \left[-\frac{h^{2}}{3} \hat{\psi}^{a(1)}(t) + \frac{4}{15} h^{2} \hat{\psi}^{a(3)}(t) \right] = 0, \tag{57}$$

$$\mathbf{N}(\mathbf{x}^{i})\mathbf{K2}(\mathbf{x}^{i}) \sum_{a=1}^{s} \mathbf{P}^{a}(\mathbf{x}^{i}) \left[-\frac{2}{3} h^{3} \hat{\psi}^{a(0)}(t) + \frac{4}{15} h^{3} \hat{\psi}^{a(2)}(t) \right] = 0, \tag{58}$$

$$\mathbf{N}(\mathbf{x}^{i})\mathbf{K2}(\mathbf{x}^{i}) \sum_{a=1}^{s} \mathbf{P}^{a}(\mathbf{x}^{i}) \left[-\frac{1}{5} h^{4} \hat{\psi}^{a(1)}(t) + \frac{4}{35} h^{4} \hat{\psi}^{a(3)}(t) \right] = 0. \tag{59}$$

The problem can be significantly simplified if both electrical displacements D_3^+ and D_3^- on the top and bottom plate surfaces are vanishing. From eq. (47) it follows directly

$$\hat{\psi}^{a(0)} = \frac{2}{3} \hat{\psi}^{a(2)}, \tag{60}$$

provided that $\det(M_2^{\cdot\cdot}) \neq 0$, where $M_2^{ai} := \left(\int\limits_{\partial\Omega_s^i} \mathbf{N}(\mathbf{x})\mathbf{K2}(\mathbf{x})\mathbf{P}^{a}(\mathbf{x}) d\Gamma(\mathbf{x}) \right)$.

For vanishing in-plane deformations the unknown linear parameter $\hat{\psi}^{a(1)}$ has to equal zero as it follows from eq. (45) provided that $\det(M_1^{\cdot\cdot}) \neq 0$, where $M_1^{ai} := \left(\int\limits_{\partial\Omega_s^i} \bar{\mathbf{N}}(\mathbf{x})\mathbf{F}(\mathbf{x})\phi^{a}(\mathbf{x}) d\Gamma(\mathbf{x}) \right)$. Of course, the mentioned determinants are different from zero as long as the unique solution exists for the considered problem.

Then, from eq. (48) it follows, that $\hat{\psi}^{a(3)} = 0$ provided that $\det(M_2^{\cdot\cdot}) \neq 0$. The system of equations (45)-(50) is reduced for this special case into the following

equations:

$$\frac{2}{3}h^3\sum_{a=1}^{s}\left(\int_{\Omega_s^i}\mathbf{W}^*(\mathbf{x})\mathbf{C}(\mathbf{x})\mathbf{B}^a(\mathbf{x})d\Omega\right)\hat{\mathbf{u}}^{a(1)}(t)$$

$$+\frac{4}{3}h\sum_{a=1}^{s}\left(\int_{\Omega_s^i}\mathbf{W}^*(\mathbf{x})\mathbf{F}(\mathbf{x})\phi^a(\mathbf{x})d\Omega\right)\hat{\psi}^{a(2)}(t)$$

$$-2h\sum_{a=1}^{s}\left(\int_{\Omega_s^i}w^*(\mathbf{x})\rho(\mathbf{x})\phi^a(\mathbf{x})d\Omega\right)\ddot{\hat{u}}_3^{a(0)}(t)+\int_{\Omega_s^i}\left[\sigma_{33}^+-\sigma_{33}^-\right]w^*(\mathbf{x})d\Omega=0, \tag{61}$$

$$-\sum_{a=1}^{s}\left(\int_{\partial\Omega_s^i}\mathbf{N}(\mathbf{x})\mathbf{K2}(\mathbf{x})\mathbf{P}^a(\mathbf{x})d\Gamma\right)\frac{8}{45}h\hat{\psi}^{a(2)}(t)$$

$$-\frac{4}{3}h\sum_{a=1}^{s}\left(\int_{\Omega_s^i}\mathbf{G}_3(\mathbf{x})\mathbf{B}3^a(\mathbf{x})d\Omega\right)\hat{\mathbf{u}}^{a(1)}(t)$$

$$+\frac{8}{3h}\sum_{a=1}^{s}\left(\int_{\Omega_s^i}k_{33}(\mathbf{x})\phi^a(\mathbf{x})d\Omega\right)\hat{\psi}^{a(2)}(t)=0, \tag{62}$$

In the system of equations (61) and (62) we have only three unknowns, namely two rotations $\hat{u}_1^{a(1)}$, $\hat{u}_2^{a(1)}$ and the potential parameter $\hat{\psi}^{a(2)}$.

If the electric potential is prescribed on the plate surfaces as $\psi(\mathbf{x},\pm h,t)=\bar{\psi}^{\pm}(\mathbf{x},t)$, it is necessary to express $D_3^{\pm}=D_3(\mathbf{x},\pm h,t)$ in terms of nodal unknowns by using

$$D_3(\mathbf{x},x_3,t)=\mathbf{G}_3(\mathbf{x})\sum_{a=1}^{s}\mathbf{B}3^a(\mathbf{x})\left[\hat{\mathbf{u}}^{a(0)}(t)+x_3\hat{\mathbf{u}}^{a(1)}(t)\right]$$
$$-\frac{k_{33}(\mathbf{x})}{2h}\left[\bar{\psi}^+(\mathbf{x},t)-\bar{\psi}^-(\mathbf{x},t)\right]$$

in the domain integrals in eqs. (47) and (48).

Collecting the discretized local boundary-domain integral equations together with the discretized boundary conditions for the displacements and potential, one obtains a complete system of ordinary differential equations and it can be rearranged in

such a way that all known quantities are on the r.h.s. Thus, in the matrix form, the system becomes

$$\mathbf{A}\ddot{\mathbf{x}} + \mathbf{C}\mathbf{x} = \mathbf{Y}. \tag{63}$$

Recall that the system matrix has a block structure. There are many time integration procedures for solution of this system of ordinary differential equations. In the present work, the Houbolt method is applied. In the Houbolt finite-difference scheme [Houbolt (1950)], the "acceleration" $\ddot{\mathbf{x}}$ is expressed as

$$\ddot{\mathbf{x}}_{\tau+\Delta\tau}^{=} \frac{2\mathbf{x}_{\tau+\Delta\tau} - 5\mathbf{x}_{\tau} + 4\mathbf{x}_{\tau-\Delta\tau} - \mathbf{x}_{\tau-2\Delta\tau}}{\Delta\tau^2}, \tag{64}$$

where $\Delta\tau$ is the size of the time-step.

Substituting eq. (61) into eq. (60), we obtain the following system of algebraic equations for the unknowns $\mathbf{x}_{\tau+\Delta\tau}$

$$\left[\frac{2}{\Delta\tau^2}\mathbf{A} + \mathbf{C}\right]\mathbf{x}_{\tau+\Delta\tau} = \frac{1}{\Delta\tau^2}5\mathbf{A}\mathbf{x}_{\tau} + \mathbf{A}\frac{1}{\Delta\tau^2}\left\{-4\mathbf{x}_{\tau-\Delta\tau} + \mathbf{x}_{\tau-2\Delta\tau}\right\} + \mathbf{Y}. \tag{65}$$

The value of the time-step has to be appropriately selected with respect to material parameters (elastic wave velocities) and time dependence of the boundary conditions.

3 Numerical examples

In this section, numerical results are presented for piezoelectric plates under a mechanical and/or electrical load. In order to test the accuracy, the numerical results obtained by the present method are compared with the results provided by the FEM-ANSYS code using a very fine mesh. In all numerical calculations, the plates with homogeneous properties are considered. We first consider a clamped square plate with a side-length $a = 0.254m$ and the plate thicknesses $2h/a = 0.05$. The origin of the coordinate system for x_3 is localized in the midplane of the plate. In the first case, on the top surface of the plate, a pure mechanical load with a uniform distribution and intensity $\sigma_{33}^{+} = 2.07 \cdot 10^6 N/m^2$ is considered. The bottom surface is kept at vanishing mechanical load. Both the top and bottom surfaces are kept at vanishing electrical displacements, $D_3^{+} = D_3^{-} = 0$. Material properties correspond to the PZT ceramic [Mitchell and Reddy (1995)] with

$$c_{11} = c_{22} = 14.8 \times 10^{10} Nm^{-2}, \quad c_{12} = 7.62 \times 10^{10} Nm^{-2},$$

$$c_{13} = c_{23} = 7.42 \times 10^{10} Nm^{-2},$$

$c_{44} = c_{55} = 2.54 \times 10^{10} Nm^{-2}$, $c_{66} = 3.59 \times 10^{10} Nm^{-2}$,

$e_{31} = e_{32} = -2.1\, Cm^{-2}$, $e_{33} = 9.5\, Cm^{-2}$,

$k_{11}/k_0 = k_{22}/k_0 = 460$, $k_{33}/k_0 = 235$, $k_0 = 8.85 \times 10^{-12} C^2/Nm^2$

$\rho = 7500 kg/m^3$.

In our numerical calculations, 441 nodes with a regular distribution were used for the approximation of 9 variables $u_j^{(0)}$, $u_\alpha^{(1)}$, $\psi^{(0)}$, $\psi^{(1)}$, $\psi^{(2)}$, $\psi^{(3)}$ (Fig. 2, where w stands for $u_3(\mathbf{x}, x_3 = 0, t) = u_3^{(0)}(\mathbf{x}, t)$). The variation of the deflection with the x_1-coordinate at $x_2 = a/2$ of the plate is presented in Fig. 3. The deflection value is normalized by the corresponding central deflection of the same elastic plate $w_3^{elast}(a/2) = 0.475 \cdot 10^{-3} m$ with vanishing piezoelectric parameters. The numerical results are compared with the results obtained by the FEM-ANSYS code 3-D analysis with a fine mesh of (4x40x40) solid 20-node elements. Four elements are considered along the thickness of the plate. Our numerical results are in a good agreement with those obtained by the FEM. One can observe that the deflection value is slightly reduced for the piezoelectric plate with respect to the elastic plate (vanishing piezoelectric parameters).

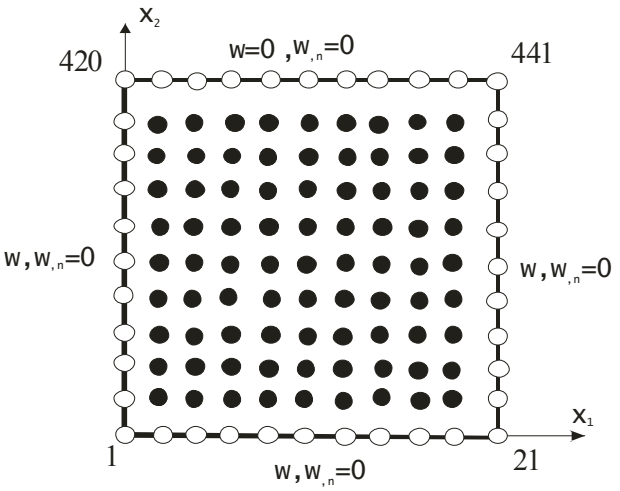

Figure 2: Node distribution for numerical analyses of a clamped square plate

The variations of the electric potential along the x_1-coordinate in the mid plane and along the thickness of the plate at its center ($x_1 = x_2 = a/2$) are presented in Figs. 4 and 5. One can see again a good agreement of results obtained by the present

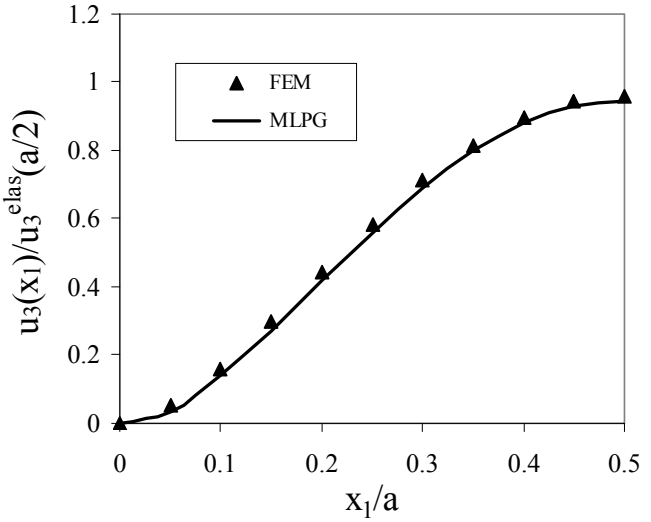

Figure 3: Variation of the deflection with the x_1-coordinate for a clamped square plate under a uniform static load

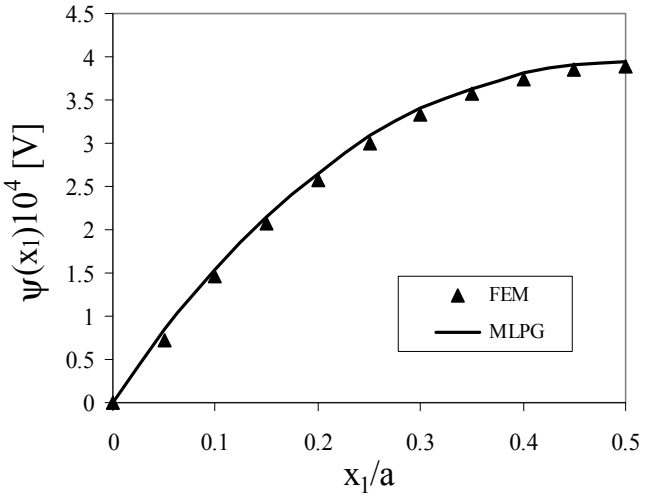

Figure 4: Variation of the potential with the x_1-coordinate for a clamped square plate under a uniform static load

MLPG and FEM methods. Relative errors of potentials in each point with respect to FEM results are less than 2%.

In the next numerical example we have considered a pure electrical charge load on the top of the plate, $D_3^+ = 1C/m^2$, and $D_3^- = 0$. The deflection value is normalized by the same central deflection $w_3^{elast}(a/2) = 0.475 \cdot 10^{-3} m$ as in the previous case for the pure mechanical load to compare influences of mechanical and electrical loads. Numerical results are presented in Fig. 6. One can see that considered electrical charge is leading to significantly higher deflections than in the case of the pure mechanical load. The MLPG numerical results are again compared with FEM ones and a good agreement is received. The variation of the electrical potential in the mid plane of the plate along the x_1 coordinate is presented in Fig. 7. Small discrepancies of the MLPG and FEM results are observed in the vicinity of the plate center but they are smaller than 4%.

Next, the piezoelectric square plate under an impact load is analyzed. The top surface of the plate is under uniform impact pure mechanical compression load with Heaviside time variation, $\sigma_{33}^+ = -2.07 \times 10^6 H(t-0) N/m^2$. The geometrical and material parameters are the same as in the static case. For the numerical modelling we have used again 441 nodes with a regular distribution. Numerical calculations are carried out for a time-step $\Delta\tau = 0.1 \times 10^{-4} s$. The time variation of the central deflection is given in Fig. 8. The results for the pure elastic and piezoelectric plates are compared there. The MLPG results are compared with those obtained by FEM-ANSYS computer code 3-D analysis with 3600 solid 20-node elements and 200 time steps. One can observe a good agreement between the FEM and MLPG results for the pure elastic plate. Since the mass density and elastic material parameters are the same for both the pure elastic and piezoelectric plates, the wave velocity is also the same in both plates. Therefore, the peaks of the deflection amplitudes are at the same time instants. A small amplification of the deflection is observed for the pure elastic plate.

Next, the simply supported piezoelectric square plate is analyzed. The geometrical and material parameters are the same as for the clamped plate. The variation of the deflection with the x_1-coordinate at $x_2 = a/2$ of the plate is presented in Fig. 9. The deflection value is normalized by the corresponding central deflection of the same elastic plate $w_3^{elast}(a/2) = 1.47 \times 10^{-3} m$ with vanishing piezoelectric parameters. The numerical results are compared with the results obtained by the FEM-ANSYS code with a fine mesh of (4x40x40) solid 20-node elements. To analyze the influence of piezoelectric parameter on the plate deflection, we have considered also $e_{31} = e_{32} = -5.1 Cm^{-2}$. One can see that smaller deflections are achieved for the plate with higher piezoelectric parameter.

Finally, the piezoelectric simply supported plate under an impact load is analyzed.

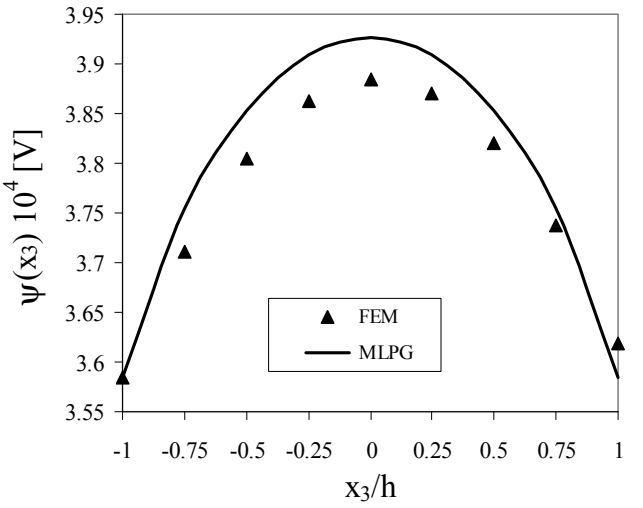

Figure 5: Variation of the potential along the thickness of the clamped square plate at $x_1 = x_2 = a/2$

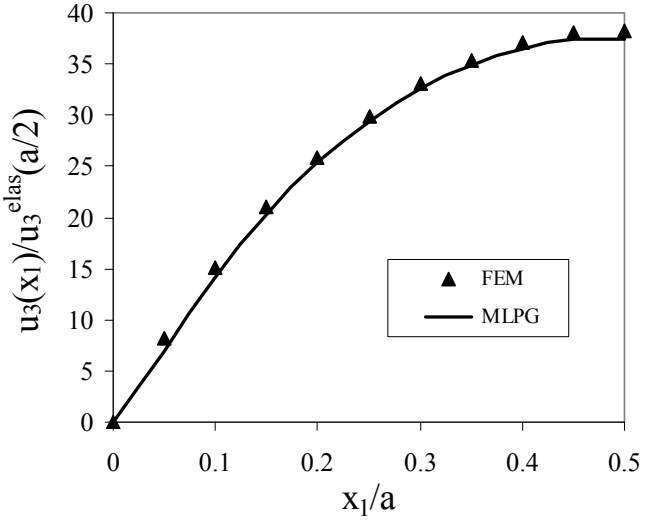

Figure 6: Variation of the deflection with the x_1-coordinate for a pure electrical charge load

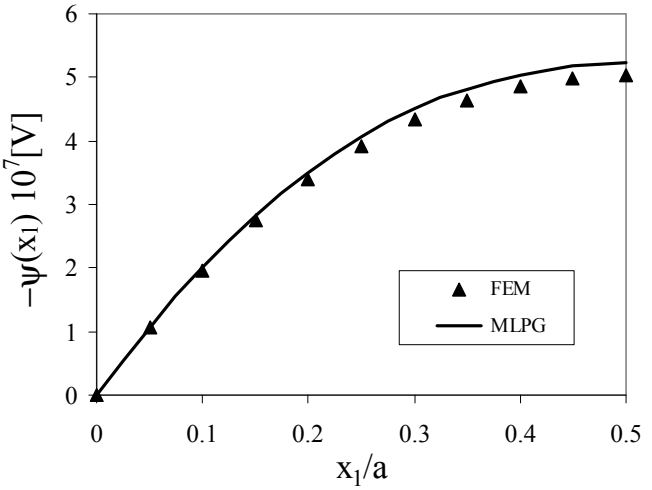

Figure 7: Variation of the potential with the x_1-coordinate for a pure electrical charge load

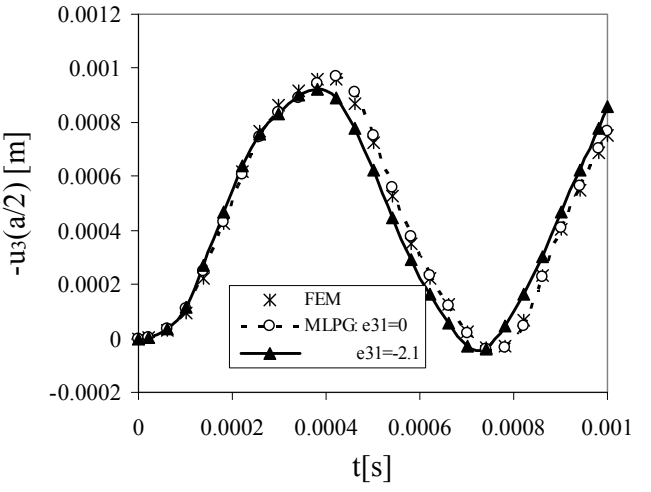

Figure 8: Time variation of the deflection at the center of a clamped piezoelectric plate subjected to a suddenly applied load

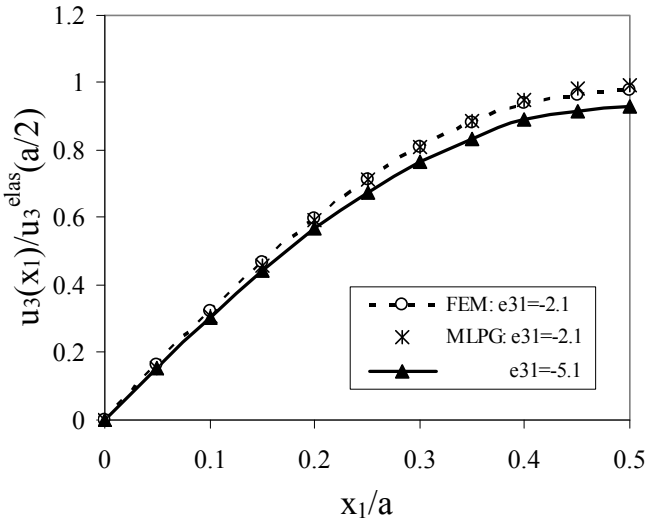

Figure 9: Variation of the deflection with the x_1 -coordinate for a simply supported piezoelectric plate under a uniform static load

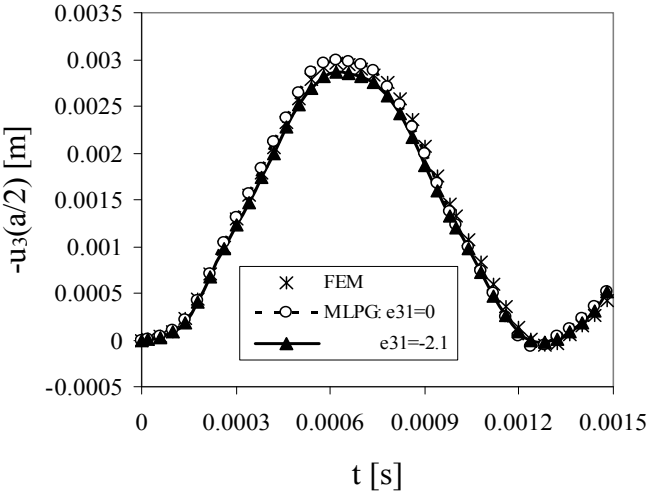

Figure 10: Time variation of the deflection at the center of a simply supported piezoelectric plate subjected to a suddenly applied load

The top surface of the plate is under uniform impact pure mechanical compression load with Heaviside time variation, $\sigma_{33}^{+} = -2.07 \times 10^6 H(t-0) N/m^2$. Numerical calculations are carried out for a time-step $\Delta\tau = 0.2 \times 10^{-4} s$. The time variation of the central deflection is given in Fig. 10. One can observe a good agreement between the FEM and MLPG results for the pure elastic plate. The plate deflection is only slightly reduced for a finite value of the piezoelectric parameter with respect to the pure elastic plate.

4 Conclusions

A meshless local Petrov-Galerkin method is applied to piezoelectric plates under a mechanical or electrical load. The governing equations for the mid-plane of the plate are derived on the base of an appropriate expansion of the mechanical displacement and electric potential in powers of the thickness coordinate in the variational equations of electroelasticity and integration through the thickness. Thus, the original 3-D thick plate problem is reduced to a 2-D problem. Nodal points are randomly distributed over the mean surface of the considered plate. Each node is the center of a circle surrounding this node. The weak forms on the small subdomains with a Heaviside step function and the radial basis function as the test functions are applied to derive local integral equations. After performing the spatial MLS approximation, a system of ordinary differential equations for the nodal unknowns is obtained. The corresponding system of the ordinary differential equations of the second order resulting from the equations of motion is solved by the Houbolt finite-difference scheme as a time-stepping method.

The proposed method is truly meshless, which requires neither domain elements nor background cells in either the interpolation or the integration. Numerical tests demonstrate a very good quality of the results obtained by the proposed MLPG method for both clamped and simply supported plates. The method is applicable for a general plate geometry and arbitrary load distribution. Successful application of the MLPG for bending of piezoelectric plates can be further extended to laminated plates and also for magneto-electro-elastic plates in future.

Acknowledgement: The authors gratefully acknowledge the support by the Slovak Science and Technology Assistance Agency registered under number APVV-0427-07 and the Slovak Grant Agency VEGA-2/0039/09.

References

Atluri S.N., Zhu T. (1998): A new Meshless Local Petrov-Galerkin (MLPG) approach in computational mechanics. *Computational Mechanics*22: 117-127.

Atluri S.N., Sladek J., Sladek V., Zhu T. (2000): The local boundary integral equation (LBIE) and its meshless implementation for linear elasticity. *Computational Mechanics*25: 180-198.

Atluri S.N. (2004): *The Meshless Method, (MLPG) For Domain & BIE Discretizations* Tech Science Press.

Atluri S.N., Han Z.D., Shen S. (2003): Meshless local Petrov-Galerkin (MLPG) approaches for solving the weakly-singular traction & displacement boundary integral equations. *CMES: Computer Modeling in Engineering & Sciences*4: 507-516.

Batra R.C., Vidoli S. (2002): Higher-order piezoelectric plate theory derived from a three-dimensional variational principle. *AIAA Journal*40: 91-104.

Belytschko T., Krogauz Y., Organ D., Fleming M., Krysl P. (1996): Meshless methods; an overview and recent developments. *Comp. Meth. Appl. Mech. Engn.* 139: 3-47.

Berlingcourt D.A., Curran D.R., Jaffe H. (1964): Piezoelectric and piezomagnetic materials and their function in transducers. *Physical Acoustics* 1: 169-270.

Han Z.D., Rajendran A.M., Atluri S.N. (2005): Meshless Local Petrov-Galerkin (MLPG) approaches for solving nonlinear problems with large deformations and rotations. *CMES: Computer Modeling in Engineering & Sciences* 0: 1-12.

Houbolt J.C. (1950): A recurrence matrix solution for the dynamic response of elastic aircraft. *Journal of Aeronautical Sciences* 7: 371-376.

Lammering R. (1991): The application of a finite shell element for composites containing piezoelectric polymers in vibration control. *Computers & Structures* 14: 1101-1109.

Lancaster P., Salkauskas T. (1981): Surfaces generated by moving least square methods. *Math. Comput.*, 37: 141-158.

Landau L.D., Lifshitz E.M. (1984): In: Lifshitz EM, Pitaevskii LP (Eds.) *Electrodynamics of Continuous Media* (Second Edition). Pergamon Press, New York.

Lee C.K. (1990): Theory of laminated piezoelectric plates for the design of distributed sensors/actuators, Part I governing equations and reciprocal relationships. *J. Accustical Soc. Am.* 87: 1144-1158.

Lee C.K., Moon F.C. (1990): Modal sensors/actuators. *J. Applied Mechanics* 57: 434-441.

Lee P.C.Y., Syngellakis S., Hou J.P. (1987): A two-dimensional theory for high-frequency vibrations of piezoelectric crystal plates with or without electrodes. *J. Applied Physics* 61: 1249-1262.

Lerch R. (1990): Simulation of piezoelectric devices by two- and three-dimensional

finite elements. *IEEE Trans. Ultrason. Ferroelec. Freq. Control* 37: 233-247.

Liu G.R., Dai K.Y., Lim K.M., Gu Y.T. (2002): A point interpolation mesh free method for static and frequency analysis of two-dimensional piezoelectric structures. *Computational Mechanics* 29: 510-519.

Liu H.T., Han Z.D., Rajendran A.M., Atluri S.N. (2006): Computational modelling of impact response with the RG damage model and the meshless local **Petrov-Galerkin** (MLPG) approaches. *CMC: Computers, Materials & Continua* 4: 43-53.

Long S.Y., Atluri S.N. (2002): A meshless local Petrov Galerkin method for solving the bending problem of a thin plate. *CMES: Computer Modeling in Engineering & Sciences*, 3: 11-51.

Mitchell J.A., Reddy J.N. (1995): A refined hybrid plate theory for composite laminates with piezoelectric laminate. *Int. J. Solids Structures* 16: 2345-2367.

Mikhailov S.E. (2002): Localized boundary-domain integral formulations for problems with variable coefficients. *Eng. Analysis with Boundary Elements* 26: 681-690.

Mindlin R.D. (1955): *An Introduction to the Mathematical Theory of the Vibrations of Elastic Plates*. U.S. Army Signal Corps Eng. Lab., Ford Monmouth, NJ.

Mindlin R.D. (1972): High frequency vibrations of piezoelectric crystal plates. *Int. J. Solids Structures* 8: 895-906.

Nayroles B., Touzot G., Villon P. (1992): Generalizing the finite element method. *Computational Mechanics*, 10: 307-318.

Ohs R.R., Aluru N.R. (2001): Meshless analysis of piezoelectric devices. *Computational Mechanics* 27: 23-36.

Parton V.Z., Kudryavtsev B.A. (1988): *Electromagnetoelasticity, Piezoelectrics and Electrically Conductive Solids.* Gordon and Breach Science Publishers, New York.

Qian, L.F., Batra, R.C., Chen, L.M. (2004):: Analysis of cylindrical bending thermoelastic deformations of fuctionally graded plates by a meshless local Petrov-Galerkin method. *Computational Mechanics*, 33: 263-273.

Reddy J.N. (2004): *Mechanics of Laminated Composite Plates and Shells*. 2^{nd} edition, CRC, Boca Raton.

Saravanos D.A., Heyliger P.R., Hopkins D.A. (1997): Layerwise mechanics and finite element for the dynamic analysis of piezoelectric composite plates. *Int. J. Solids Structures* 34: 359-378.

Sellountos E.J., Vavourakis V., Polyzos D. (2005): A new singular/hypersingular **MLPG** (LBIE) method for 2D elastostatics. *CMES: Computer Modeling in Engi-*

neering & Sciences 7: 35-48.

Sladek J., Sladek V., Atluri S.N. (2004): Meshless local Petrov-Galerkin method in anisotropic elasticity. *CMES: Computer Modeling in Engineering & Sciences* 6, 477-489.

Sladek J., Sladek V., Zhang Ch., Garcia-Sanchez F., Wunsche M. (2006a): Meshless local Petrov-Galerkin method for plane piezoelectricity. *CMC: Computers, Materials & Continua* 4, 109-118.

Sladek J., Sladek V., Wen P.H., Aliabadi M.H. (2006b): Meshless Local **Petrov-Galerkin** (MLPG) method for shear deformable shells analysis, *CMES: Computer Modeling in Engineering & Sciences* 13, 103-118.

Sladek J., Sladek V., Zhang Ch., Solek P. (2007a): Application of the MLPG to thermo-piezoelectricity. *CMES: Computer Modeling in Engineering & Sciences* 22: 217-233.

Sladek J., Sladek V., Zhang Ch., Solek P., Pan E. (2007b): Evaluation of fracture parameters in continuously nonhomogeneous piezoelectric solids. *Int. J. Fracture* 145: 313–326.

Sladek J., Sladek V., Krivacek J., Wen P.H., Zhang Ch. (2007c): Meshless Local **Petrov-Galerkin** (MLPG) method for Reissner-Mindlin plates under dynamic load. *Computer Meth. Appl. Mech. Engn.* 196: 2681-2691.

Sladek J., Sladek V., Solek P., Pan E. (2008): Fracture analysis of cracks in magneto-electro-elastic solids by the MLPG. *Computational Mechanics* 42: 697-714.

Soric J., Li Q., Atluri S.N. (2004): Meshless local Petrov-Galerkin (MLPG) formulation for analysis of thick plates. *CMES: Computer Modeling in Engineering & Sciences* 6: 349-357.

Tiersten H.F., Mindlin R.D. (1962): Forced vibrations of piezoelectric crystal plates. *Quartely of Applied Mathematics* 20: 107-119.

Tiersten H.F. (1969): *Linear Piezoelectric Plate Vibrations*. Plenum Press, New York.

Tzou H.S., Tseng C.I. (1990): Distributed piezoelectric sensor/actuator design for dynamic measurement/control of distributed parametric systems: A piezoelectric finite element approach. *J. Sound Vibration* 138: 17-34.

Vavourakis V., Polyzos D. (2007): A MLPG4 (LBIE) formulation in elastostatics. *CMC: Computers, Materials & Continua* 5: 185-196.

Vel S.S., Batra R.C. (2000): Three-dimensional analytical solution for hybrid multilayered piezoelectric plates. *J. Applied Mechanics* 67: 558-567.

Yang J.S. (1999): Equations for the extension and flexure of electroelastic plates under strong electric fields. *Int. J. Solids Structures* 36: 3171-3192.

Yong Y.K., Stewart J.T. (1991): Mass-frequency influence surface, node shapes, and frequency spectrum of a rectangular AT-cut quartz plate. *IEEE Trans. Ultrason. Ferroelec. Freq. Control* 38: 67-73.

Wang J., Yang J. (2000): Higher-order theories of piezoelectric plates and applications. *Applied Mechanics Reviews* 53: 87-99.

CMES: Computer Modeling in Engineering & Sciences

ISSN : 1526-1492 (Print); 1526-1506 (Online)

Journal website:
http://www.techscience.com/cmes/

Manuscript submission
http://submission.techscience.com

Published by
Tech Science Press
5805 State Bridge Rd, Suite G108
Duluth, GA 30097-8220, USA

Phone (+1) 678-392-3292
Fax (+1) 678-922-2259
Email: sale@techscience.com
Website: http://www.techscience.com
Subscription: http://order.techscience.com

CMES is Indexed & Abstracted in
Applied Mechanics Reviews; Cambridge Scientific Abstracts (Aerospace and High Technology; Materials Sciences & Engineering; and Computer & Information Systems Abstracts Database); CompuMath Citation Index; Current Contents: Engineering, Computing & Technology; Engineering Index (Compendex); INSPEC Databases; Mathematical Reviews; MathSci Net; Mechanics; Science Alert; Science Citation Index; Science Navigator; Zentralblatt fur Mathematik.